RSC Advances

PAPER

View Article Online
View Journal | View Issue

Cite this: *RSC Adv.*, 2015, **5**, 36507

Platinum(II) polymetallayne-based phosphorescent polymers with enhanced triplet energy-transfer: synthesis, photophysical, electrochemistry, and electrophosphorescent investigation†

Zuan Huang,[a] Boao Liu,[a] Jiang Zhao,[a] Yue He,[a] Xiaogang Yan,[a] Xianbin Xu,[a] Guijiang Zhou,*[a] Xiaolong Yang*[a] and Zhaoxin Wu*[b]

Received 2nd March 2015
Accepted 31st March 2015

DOI: 10.1039/c5ra03697f

www.rsc.org/advances

Two series of new phosphorescent copolymers with bicarbazole-based platinum(II) polymetallayne backbones have been successfully prepared through Sonogashira cross-coupling with different Ir^{III} ppy-type (ppy = 2-phenylpyridine anion) complexes as phosphorescent centers. The photophysical investigations not only indicate a highly efficient triplet energy-transfer process from the polymetallayne segments to the phosphorescent units in the polymer solution, but also figure out the structure–property relationship between the triplet energy-transfer process and the energy-levels of different excited states. In addition, the phosphorescent copolymers can produce yellow-emitting phosphorescent OLEDs (PHOLEDs) with high EL efficiencies and a current efficiency (η_L) of 11.49 cd A^{-1}, an external quantum efficiency (η_{ext}) of 4.38%, a power efficiency (η_P) of 3.78 lm W^{-1}, and red-emitting PHOLEDs with a η_L of 5.86 cd A^{-1}, η_{ext} of 10.1%, and a η_P of 2.29 lm W^{-1}, representing very decent electroluminescent performances achieved by the phosphorescent copolymers. Herein, this work not only furnishes very important clues for further polishing of this category novel phosphorescent polymer, but also provides a new approach to the design and synthesis of highly efficient phosphorescent copolymers.

1. Introduction

Phosphorescent polymers can properly compromise high electroluminescent (EL) efficiency and easy device fabrication.[1–3] These luminescent polymers have therefore received increasing interest in the field of organic light-emitting devices/diodes (OLEDs), since they can effectively enhance the EL efficiencies of solution-processed OLEDs compared with their fluorescent counterparts.[4,5] As the most important component in these polymers, the phosphorescent blocks, typically ppy-type iridium(III) complexes (ppy = 2-phenylpyridine anion), can either be embedded into the main chain[6–10] or attached to the backbone as side chains[11–16] of the obtained phosphorescent polymers. Playing the same role of the host materials in the phosphorescent OLEDs with small molecular triplet emitters, the organic segments in the phosphorescent polymers can act as the host of the phosphorescent blocks. Thus, the emission layer (EML) in the PHOLEDs can be easily constructed by directly spin-coating a solution of the phosphorescent polymers, which can greatly simplify the device fabrication. Similar to their fluorescent counterparts, PHOLEDs also relate to the charge carrier injection/transporting in their EMLs. Thus, it seems that the phosphorescent polymers with conjugated backbones are preferred to promote the charge carrier injection/transporting in the EML of the PHOLEDs. Another critical issue that should be addressed in PHOLEDs based on conjugated phosphorescent polymers is blocking the undesired reverse energy-transfer from the emissive triplet states of the phosphorescent units to the non-emissive triplet states of the conjugated backbones in the phosphorescent polymers.[5] In order to achieve high EL performance in the PHOLEDs, the reverse energy-transfer process should be restrained as far as possible. Increasing the triplet energy level of the backbones of the phosphorescent polymers should be a feasible way to achieve this. Therefore, phosphorescent polymers with nonconjugated backbones have also been prepared. Clearly, this type of polymer backbone seems unfavourable for charge carrier injection/transporting. In order to overcome the weakness

[a]*MOE Key Laboratory for Nonequilibrium Synthesis and Modulation of Condensed Matter, State Key Laboratory for Mechanical Behavior of Materials, Institute of Chemistry for New Energy Material, Department of Chemistry, Faculty of Science, Xi'an Jiaotong University, Xi'an 710049, P.R. China. E-mail: zhougj@mail.xjtu.edu.cn; Fax: +86-29-8266-3914*

[b]*Key Laboratory of Photonics Technology for Information, School of Electronic and Information Engineering, Xi'an Jiaotong University, Xi'an 710049, P.R. China. E-mail: zhaoxinwu@mail.xjtu.edu.cn*

† Electronic supplementary information (ESI) available. See DOI: 10.1039/c5ra03697f

associated with the nonconjugated backbones of phosphorescent polymers, functional moieties, such as aromatic silane, have been introduced into the polymer backbone to furnish a high triplet energy level.[17] Despite of all these endeavours, only a handful of phosphorescent polymers with judicious molecular design can show a good performance.[16,18,19] Furthermore, most of them still show much lower EL efficiencies compared with small molecular triplet emitters involved in PHOLEDs made by a vacuum deposition method.[20] So, novel molecular designs are really needed to further polish the EL performance of the phosphorescent polymers.

From what is mentioned above, one might conclude that maintaining the optimized trade-offs between high triplet energy level and good charge carrier injection/transporting of the backbones should represent an effective strategy to enhance the EL capacity of the phosphorescent polymers. For an organic conjugated backbone, a twisted configuration should be required to furnish a high triplet energy level. Obviously, it should not favour charge carrier transporting by the hopping mechanism. Maybe it is time to broke away from conventions and develop new phosphorescent polymers based on totally different backbones. Recently, owing to their diverse photophysical properties, platinum(II) polymetallaynes have found important applications in optical power limiting[21,22] and photovoltaics,[23,24] *etc.* In addition, some bithiazole-based platinum(II) polymetallaynes can serve as fluorescent emitters in OLEDs.[25] Different from the π–π conjugations in backbones of the traditional conjugated polymers, *i.e.* polymers with pure organic or metal-free conjugated backbones,[5] the d–π conjugation between platinum(II) ions and the organic spacers,[26–28] *i.e.* aromatic alkynes, shows a relatively weaker conjugation extending ability to furnish the backbones of the platinum(II) polymetallaynes with a high triplet energy level.[29] Meanwhile, the conjugation of the backbones of platinum(II) polymetallaynes can be maintained to benefit charge carrier injection/transporting. Hence, platinum(II) polymetallaynes should show great potential to overcome the drawbacks associated with the traditional conjugated phosphorescent polymers, which has been shown by our recent preliminary results.[30] The concerned novel phosphorescent polymers with platinum(II) polymetallayne backbone can show high EL performance with a current efficiency (η_L) of 9.17 cd A^{-1}.[30] It is well accepted that the energy-transfer from the polymer backbones to the phosphorescent units can play a critical role in determining the EL performances of the concerned phosphorescent polymers. Thus, optimizing the energy-transfer processes aforementioned in this novel kind of phosphorescent polymer should be of great importance in obtaining the structure–property relationship information to provide valuable clues for the design and synthesis of new high-performance phosphorescent polymers. So, in this paper, two series of phosphorescent polymers with bicarbazole-based platinum(II) polymetallayne backbones and ppy-type iridium(III) phosphorescent centers have been developed (Chart 1). It was found that the energy-transfer from the polymetallayne backbones to the phosphorescent blocks could be greatly affected by the triplet energy-level difference between the backbone and phosphorescent center, which will indicate important information of the structure–property relationship of these novel phosphorescent polymers. Furthermore, the results also provide valuable clues to optimize the EL performances of these phosphorescent polymers.

2. Experimental section

2.1. General information

The commercially available reagents were used directly as received unless otherwise stated. All reactions proceeded under an inert atmosphere. The solvents were purified by standard methods under dry nitrogen before use. The reactions were monitored using thin-layer chromatography (TLC) with Merck pre-coated aluminum plates. Flash column chromatography and preparative TLC were carried out using silica gel for small molecular compounds. All Sonogashira copolymerization reactions were carried out with Schlenk techniques under a nitrogen atmosphere.

2.2. Physical characterization

^{1}H NMR and ^{13}C NMR spectra were measured in $CDCl_3$ using a Bruker AXS 400 MHz spectrometer with the chemical shifts quoted relative to tetramethylsiliane (TMS). Fast atom bombardment (FAB) mass spectra were recorded on a Finnigan MAT SSQ710 system. UV-Vis spectra were recorded using a Shimadzu UV-2250 spectrophotometer. The photoluminescent (PL) properties of the copolymers were measured using an Edinburgh Instruments FLS920 spectrophotometer. The lifetimes for the excited states were measured using a single photon counting spectrometer from Edinburgh Instruments FLS920 with a 360 nm picosecond LED lamp as the excitation source, while those at 77 K were obtained using excitation from a xenon flash lamp. Differential scanning calorimetry (DSC) was performed with a NETZSCH DSC 200 PC unit under a nitrogen flow at a heating rate of 10 °C min^{-1}. Thermogravimetric analysis (TGA) was conducted with a NETZSCH STA 409C instrument under nitrogen with a heating rate of 20 °C min^{-1}. The molecular weights of the copolymers were determined using Waters 2695 GPC in THF. The weights were estimated using a calibration curve of polystyrene standards. Cyclic voltammetry (CV) measurement for the sample solution was performed on a Princeton Applied Research model 2273A potentiostat with a glassy carbon working electrode, a platinum counter electrode, and a platinum-wire reference electrode at a scan rate of 100 mV s^{-1}. The solvent was deoxygenated dichloromethane, and the supporting electrolyte was 0.1 M [nBu$_4$N][BF_4]. Ferrocene (Fc) was added as an internal calibrant for the measurement, and all potentials reported were quoted with reference to the Fc–Fc^+ couple. The polymer films on a quartz substrate were obtained by spin-coating their chlorobenzene solution (*ca.* 20 mg mL^{-1}), and their thickness was determined by a Nanoview SE MF-1000 Ellipsometer. The PL spectra and lifetimes at 77 K were obtained by dipping the degassed sample CH_2Cl_2 solution in a thin quartz tube into

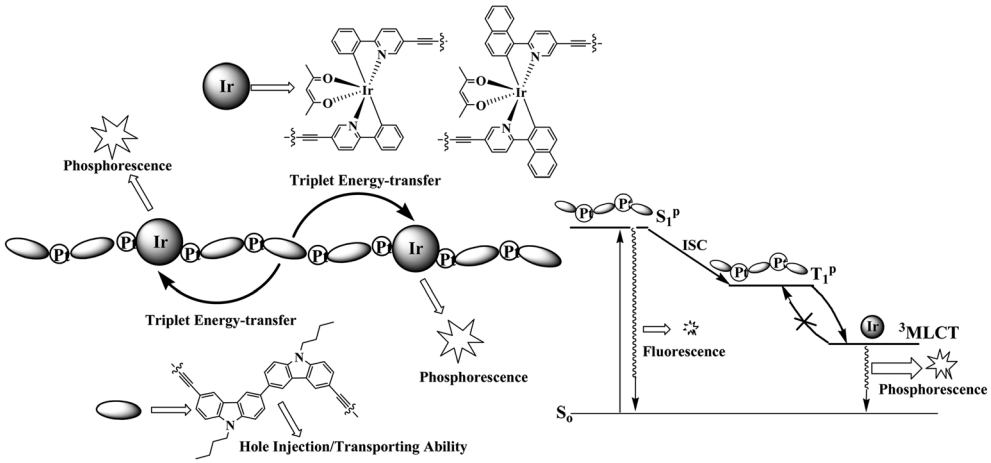

Chart 1 The schematic diagram of the chemical structure of the novel phosphorescent polymers and a sketch of the energy-transfer process involved.

liquid nitrogen Dewar and the data was recorded after standing for 3 minutes.

2.3. Synthesis

The synthetic details of the key compounds **L1** and **L2**, organic monomer **MC**, **IrBr1**, **IrBr2** and the model polymer **P-BC** are presented in the ESI.†

IrSi1. To the mixture of **IrBr1** (0.76 g, 1.00 mmol), $Pd(PPh_3)_2Cl_2$ (20 mg, 0.071 mmol), CuI (13 mg, 0.071 mmol) and Et_3N/CH_2Cl_2 (30 mL, v/v = 1 : 1), trimethylsilylacetylene (0.5 mL) was added at room temperature. After stirring for one hour at room temperature, the reaction mixture was allowed to proceed at 70 °C for 30 h. After cooling to room temperature, the reaction mixture was concentrated under a vacuum to give the crude product, which was further purified by silica gel column chromatography with petroleum ether/CH_2Cl_2 (1 : 1, v/v) as the eluent to obtain the pure product as an orange solid (0.60 g, 75.8%). ^{1}H NMR 8.56 (s, 2H), 7.76 (s, 4H), 7.52 (d, J = 7.6 Hz, 2H), 6.79 (t, J = 7.2 Hz, 2H), 6.70 (t, J = 7.2 Hz, 2H), 6.25 (d, J = 7.6 Hz, 2H), 5.26 (s, 1H), 1.81 (s, 6H), 0.27 (s, 9H); ^{13}C NMR (100 MHz, $CDCl_3$, δ, ppm): 184.90, 168.12, 151.10, 148.55, 143.99, 133.12, 129.69, 124.52, 120.99, 117.67, 100.98, 100.82, 98.88, 31.61, 28.81, 22.68, 14.16, −0.19; FAB-MS (m/z): 792 $[M]^+$. Elemental analysis calcd (%) for $C_{37}H_{39}IrN_2O_2Si_2$: C 56.10, H 4.96, N 3.54; found: C 56.39, H 4.75, N 3.38.

IrM1. The solution of tetrabutylammonium fluoride trihydrate (80 mg, 0.25 mmol) in CH_2Cl_2 (3 mL) was added to the mixture of **IrSi1** (0.10 g, 0.13 mmol) and CH_2Cl_2 (15 mL). After stirring 30 min at room temperature, the reaction mixture was washed with water (3 × 20 mL). The organic phase was dried over $MgSO_4$ and passed through a short silica gel pad quickly. After concentration, the residue was precipitated in hexane. The product was obtained as an orange-red solid (72 mg, 85.9%). ^{1}H NMR (400 MHz, $CDCl_3$, δ, ppm): 8.59 (s, 2H), 7.79 (s, 4H), 7.52 (d, J = 7.8 Hz, 2H), 6.83 (t, J = 7.8 Hz, 2H), 6.72 (t, J = 7.2 Hz, 2H), 6.26 (d, J = 7.6 Hz, 2H), 5.26 (s, 1H), 3.27 (s, 2H), 1.82 (s, 6H); ^{13}C NMR (100 MHz, $CDCl_3$, δ, ppm): 184.95, 168.62, 151.15, 148.53, 143.84, 140.04, 133.12, 129.77, 124.61, 121.03, 117.73, 116.42, 100.80, 81.08, 77.20, 28.76; FAB-MS (m/z): 648 $[M]^+$. Elemental analysis calcd (%) for $C_{31}H_{23}IrN_2O_2$: C 57.48, H 3.58, N 4.32; found: C 57.27, H 3.49, N 4.18.

P-YC-1. Under a N_2 atmosphere, **MC** (95.0 mg, 0.193 mmol), **IrM1** (5.0 mg, 0.007 mmol) and *trans*-$[PtCl_2(PBu_3)_2]$ (135.0 mg, 0.20 mmol) were mixed in a solvent mixture of degassed Et_3N/CH_2Cl_2 (10 mL/20 mL) under stirring. After the monomers were completely dissolved, CuI (10 mg) was added. The mixture was stirred for 18 h at room temperature. The reaction mixture was then stirred for 5 h after adding phenylacetylene (5.0 mg, 0.05 mmol). The reaction mixture was then concentrated and precipitated in methanol. The precipitation was collected and dissolved in CH_2Cl_2. The copolymer solution was filtered using a 0.45 μm PTFE syringe filter. After concentration, the copolymer was purified by precipitation twice in methanol and washed with methanol in a Soxhlet apparatus for 72 h, and dried under a vacuum. It was obtained as a light orange solid (yield: 80%). ^{1}H NMR (400 MHz, $CDCl_3$, δ, ppm): 8.39 (s), 8.27 (s), 8.21 (s), 8.14 (s), 8.09 (s), 8.07 (s), 7.82–7.80 (m), 7.65–7.62 (m), 7.46–7.42 (m), 4.30 (br), 2.26 (br), 1.88 (br), 1.75–1.72 (br), 1.53–1.40 (m), 1.00–0.93 (m); ^{31}P NMR (161.9 MHz, $CDCl_3$, δ, ppm): 3.32, 2.82; gel permeation chromatography (GPC): number-average molecular weight (M_n) = 3.8 × 10^4 g mol^{-1}, polydispersity index (PDI) = 1.6 (against polystyrene standards).

P-YC-2. It was prepared from **MC** (90.0 mg, 0.183 mmol), **IrM1** (10.0 mg, 0.015 mmol), *trans*-$[PtCl_2(PBu_3)_2]$ (133.0 mg, 0.198 mmol) and CuI (10 mg), following the same procedure as for **P-YC-1**. The copolymer was obtained as an orange solid (yield: 83%). ^{1}H NMR (400 MHz, $CDCl_3$, δ, ppm): 8.40 (s), 8.28 (s), 8.22 (s), 8.15 (s), 8.11 (s), 8.09 (s), 7.83–7.77 (m), 7.64 (br), 7.48–7.43 (m), 4.30 (br), 2.27 (br), 1.88 (br), 1.75–1.72 (br), 1.53–1.40 (m), 1.00–0.93 (m); ^{31}P NMR (161.9 MHz, $CDCl_3$, δ, ppm): 3.24, 2.81; GPC: M_n = 3.6 × 10^4 g mol^{-1}, PDI = 1.6 (against polystyrene standards).

P-YC-3. It was prepared from **MC** (85.0 mg, 0.172 mmol), **IrM1** (15.0 mg, 0.023 mmol), *trans*-$[PtCl_2(PBu_3)_2]$ (131.0 mg, 0.195 mmol) and CuI (10 mg), following the same procedure as

for **P-YC-1**. The copolymer was obtained as an orange solid (yield: 85%). ^{1}H NMR (400 MHz, $CDCl_3$, δ, ppm): ^{1}H NMR (400 MHz, $CDCl_3$, δ, ppm): 8.39 (s), 8.28 (s), 8.22 (s), 8.15 (s), 8.10 (s), 8.08 (s), 7.83–7.77 (m), 7.64 (br), 7.47–7.43 (m), 4.30 (br), 2.27 (br), 1.88 (br), 1.75–1.72 (br), 1.53–1.40 (m), 1.00–0.93 (m); ^{31}P NMR (161.9 MHz, $CDCl_3$, δ, ppm): 3.23, 2.84; GPC: $M_n = 3.5 \times 10^4$ g mol^{-1}, PDI = 1.7 (against polystyrene standards).

P-YC-4. It was prepared from **MC** (80.0 mg, 0.162 mmol), **IrM1** (20.0 mg, 0.027 mmol), *trans*-[$PtCl_2(PBu_3)_2$] (127.0 mg, 0.189 mmol) and CuI (10 mg), following the same procedure as for **P-YC-1**. The copolymer was obtained as an orange solid (yield: 82%). ^{1}H NMR (400 MHz, $CDCl_3$, δ, ppm): 8.38 (s), 8.26 (s), 8.20 (s), 8.13 (s), 8.08 (s), 7.79–7.77 (m), 7.64 (br), 7.47–7.43 (m), 4.29 (br), 2.24 (br), 1.87 (br), 1.75–1.72 (br), 1.53–1.40 (m), 0.98–0.92 (m); ^{31}P NMR (161.9 MHz, $CDCl_3$, δ, ppm): 3.22, 2.83; GPC: $M_n = 3.3 \times 10^4$ g mol^{-1}, PDI = 1.8 (against polystyrene standards).

IrSi2. To the mixture of **IrBr2** (0.6 g, 0.70 mmol), $Pd(PPh_3)_2Cl_2$ (20 mg, 0.029 mmol) and CuI (5 mg, 0.029 mmol) and Et_3N/CH_2Cl_2 (20 mL, v/v = 1 : 1), trimethylsilylacetylene (0.5 mL) was added at room temperature. After stirring for one hour at room temperature, the reaction mixture was allowed to proceed at 70 °C for 30 h. After cooling to room temperature, the reaction mixture was concentrated under a vacuum to obtain the crude product, which was further purified using silica gel column chromatography with petroleum ether/CH_2Cl_2 (1 : 1, v/v) as the eluent to obtain the pure product as a red solid (0.45 g, 72.1%). ^{1}H NMR (400 MHz, $CDCl_3$, δ, ppm): 8.60 (s, 2H), 7.47 (t, J = 7.2 Hz, 4H), 7.83 (dd, J = 8.4, 2.0 Hz, 2H), 7.62 (d, J = 7.2 Hz, 2H), 7.46 (t, J = 7.0 Hz, 2H), 7.26 (t, J = 7.4 Hz, 2H), 7.04 (d, J = 8.4 Hz, 2H), 6.25 (d, J = 8.4 Hz, 2H), 5.31 (s, 1H), 1.83 (s, 6H), 0.27 (s, 18H); ^{13}C NMR (100 MHz, $CDCl_3$, δ, ppm): 185.14, 168.62, 157.14, 151.49, 139.64, 137.61, 132.02, 131.80, 131.17, 129.81, 129.25, 126.60, 122.49, 121.40, 121.15, 116.20, 101.02, 100.83, 98.88, 28.69, −0.20; FAB-MS (*m*/*z*): 892 $[M]^+$. Elemental analysis calcd (%) for $C_{45}H_{43}IrN_2O_2Si_2$: C 60.58, H 4.86, N 3.14; found: C 60.39, H 4.65, N 3.08.

IrM2. The solution of tetrabutylammonium fluoride trihydrate (75 mg, 0.24 mmol) in CH_2Cl_2 (3 mL) was added to the mixture of **IrSi2** (0.10 g, 0.11 mmol) and CH_2Cl_2 (15 mL). After stirring for 30 min at room temperature, the reaction mixture was washed with water (3 × 20 mL). The organic phase was dried over $MgSO_4$ and passed through a short silica gel pad quickly. After concentration, the residue was precipitated in hexane. The product was obtained as a red solid (69 mg, 82.3%). ^{1}H NMR (400 MHz, $CDCl_3$, δ, ppm): 8.63 (s, 2H), 8.49 (dd, J = 8.8, 4.0 Hz, 4H), 7.87 (d, J = 8.8 Hz, 2H), 7.62 (d, J = 8.0 Hz, 2H), 7.46 (t, J = 7.6 Hz, 2H), 7.26 (t, J = 7.4 Hz, 2H), 7.05 (d, J = 8.4 Hz, 2H), 6.28 (d, J = 8.4 Hz, 2H), 5.30 (s, 1H), 3.28 (s, 2H), 1.83 (s, 6H); ^{13}C NMR (100 MHz, $CDCl_3$, δ, ppm): 185.19, 169.22, 157.21, 151.54, 140.05, 132.01, 131.18, 129.88, 129.44, 126.69, 122.54, 121.51, 121.11, 109.99, 100.82, 81.08, 77.23, 28.74; FAB-MS (*m*/*z*): 748 $[M]^+$. Elemental analysis calcd (%) for $C_{39}H_{27}IrN_2O_2$: C 62.63, H 3.64, N 3.75; found: C 62.34, H 3.35, N 3.28.

P-RC-1. It was prepared from **MC** (95.0 mg, 0.193 mmol), **IrM2** (5.0 mg, 0.007 mmol), *trans*-[$PtCl_2(PBu_3)_2$] (134.0 mg, 0.200 mmol) and CuI (10 mg), following the same procedure as for **P-YC-1**. The copolymer was obtained as an orange solid (yield: 83%). ^{1}H NMR (400 MHz, $CDCl_3$, δ, ppm): 8.48 (s), 8.39 (s), 8.32 (s), 8.27 (s), 8.21 (s), 8.17 (s), 8.14 (s), 8.11–8.07 (br), 7.82–7.76 (m), 7.64 (br), 7.51–7.42 (m), 4.30 (br), 2.27 (br), 1.88 (br), 1.75–1.72 (br), 1.53–1.40 (m), 1.00–0.93 (m); ^{31}P NMR (161.9 MHz, $CDCl_3$, δ, ppm): 3.23, 2.83; GPC: $M_n = 3.5 \times 10^4$ g mol^{-1}, PDI = 1.5 (against polystyrene standards).

P-RC-2. It was prepared from **MC** (90.0 mg, 0.183 mmol), **IrM2** (10.0 mg, 0.013 mmol), *trans*-[$PtCl_2(PBu_3)_2$] (131.0 mg, 0.196 mmol) and CuI (10 mg), following the same procedure as for **P-YC-1**. The copolymer was obtained as an orange solid (yield: 83%). ^{1}H NMR (400 MHz, $CDCl_3$, δ, ppm): 8.48 (s), 8.39 (s), 8.32 (s), 8.28 (s), 8.21 (s), 8.17 (s), 8.14 (s), 8.11–8.07 (br), 7.82–7.76 (m), 7.65 (br), 7.51–7.42 (m), 4.30 (br), 2.27 (br), 1.88 (br), 1.75–1.72 (br), 1.53–1.40 (m), 1.00–0.93 (m); ^{31}P NMR (161.9 MHz, $CDCl_3$, δ, ppm): 3.24, 2.81; GPC: $M_n = 3.3 \times 10^4$ g mol^{-1}, PDI = 1.6 (against polystyrene standards).

P-RC-3. It was prepared from **MC** (85.0 mg, 0.172 mmol), **IrM2** (15.0 mg, 0.020 mmol), *trans*-[$PtCl_2(PBu_3)_2$] (130.0 mg, 0.192 mmol) and CuI (10 mg), following the same procedure as for **P-YC-1**. The copolymer was obtained as an orange solid (yield: 81%). ^{1}H NMR (400 MHz, $CDCl_3$, δ, ppm): 8.48 (s), 8.39 (s), 8.32 (s), 8.27 (s), 8.21 (s), 8.17 (s), 8.14 (s), 8.11–8.07 (br), 7.82–7.76 (m), 7.64 (br), 7.52–7.42 (m), 4.30 (br), 2.27 (br), 1.88 (br), 1.75–1.72 (br), 1.53–1.40 (m), 1.00–0.93 (m); ^{31}P NMR (161.9 MHz, $CDCl_3$, δ, ppm): 3.23, 2.84; GPC: $M_n = 3.4 \times 10^4$ g mol^{-1}, PDI = 1.7 (against polystyrene standards).

P-RC-4. It was prepared from **MC** (80.0 mg, 0.162 mmol), **IrM2** (20.0 mg, 0.027 mmol), *trans*-[$PtCl_2(PBu_3)_2$] (127.0 mg, 0.189 mmol) and CuI (10 mg), following the same procedure as for **P-YC-1**. The copolymer was obtained as an orange solid (yield: 82%). ^{1}H NMR (400 MHz, $CDCl_3$, δ, ppm): 8.48 (s), 8.39 (s), 8.32 (s), 8.28 (s), 8.22 (s), 8.14 (s), 8.12–8.07 (br), 7.83–7.76 (m), 7.64 (br), 7.58–7.42 (m), 4.30 (br), 2.27 (br), 1.88 (br), 1.75–1.72 (br), 1.53–1.40 (m), 1.00–0.93 (m); ^{31}P NMR (161.9 MHz, $CDCl_3$, δ, ppm): 3.22, 2.82; GPC: $M_n = 3.2 \times 10^4$ g mol^{-1}, PDI = 1.7 (against polystyrene standards).

2.4. OLED fabrication and measurements

The methods of OLED fabrication and measurements are similar to those of our previous study.[30] The pre-cleaned ITO glass substrates were treated with ozone for 20 min. Then, the PEDOT:PSS was deposited on the surface of the ITO glass by a spin-coating method to form a 45 nm-thick hole-injection layer. After being cured at 120 °C for 30 min in the air, the emitting layer (35 nm) was obtained by spin-coating a chlorobenzene solution of each phosphorescent polymer. The ITO glass was dried in a vacuum oven at 50 °C for 20 min and transferred to the deposition system for organic and metal deposition. TPBi (45 nm), LiF (1 nm) and Al cathode (100 nm) were successively evaporated at a base pressure less than 10^{-6} Torr. The EL spectra and CIE coordinates were measured with a PR650 spectra colorimeter. The *L*–*V*–*J* curves of the devices were recorded by a Keithley 2400/2000 source meter and the luminance was measured using a PR650 SpectraScan spectrometer.

All the experiments and measurements were carried out under ambient conditions.

3. Results and discussion

3.1. Synthesis and characterization

As the most critical component, the synthetic details for the phosphorescent monomers **IrM1** and **IrM2** are shown in Fig. 1. The organic ligands **L1** and **L2** were prepared by Suzuki cross-coupling between 5-bromo-2-iodopyridine and the corresponding arylboronic acid under a lower temperature (*ca.* 90 °C) in high yield. The precursor complexes **IrBr1** and **IrBr2** were prepared according to the well-established two-step strategy by the cyclometalation of $IrCl_3 \cdot nH_2O$ with the corresponding organic ligands, followed by coordination of the acetylacetone (acac) anion in the presence of Na_2CO_3. After undergoing a Sonogashira coupling reaction, **IrBr1** and **IrBr2** were converted respectively to **IrSi1** and **IrSi2**, which went through the cleaving of trimethylsilane groups to obtain **IrM1** and **IrM2** in high purity as a colored solid (Fig. 1). Serving as the aromatic spacers, the organic monomer **MC** was prepared through a Sonogashira coupling reaction between **BCBr** and trimethylsilylacetylene, followed by the trimethylsilane cleaving of **BCSi** with $[n\mathrm{Bu}_4\mathrm{N}]\mathrm{F}$ (Scheme S1 in the ESI†). Due to the excellent hole injection/transporting (HI/HT) features associated with the carbazole unit, a bicarbazole moiety was employed in **MC** with the aim to improve the EL performance of the final phosphorescent polymers.

After obtaining all the key monomers, the designed phosphorescent copolymers can be easily prepared by the Sonogashira cross-coupling procedure between the phosphorescent monomer **IrM1** or **IrM2**, organic monomer **MC** and *trans*-$[PtCl_2(PBu_3)_2]$ (Fig. 2). The amount of the yellow-emitting phosphorescent monomer **IrM1** was set to maintain its weight percentage *ca.* 2.1, 4.3, 6.5, and 8.7 wt% in the final phosphorescent polymers, corresponding to the different feed ratios of **MC** and **IrM1** as follows: $m : n = 193 : 7$ for **P-YC-1**, $m : n = 183 : 15$ for **P-YC-2**, $m : n = 172 : 23$ for **P-YC-3**, and $m : n = 162 : 27$ for **P-YC-4**, respectively (Fig. 2). Similarly, the content of the red-emitting phosphorescent monomer **IrM2** was set to weight percentages *ca.* 2.1, 4.3, 6.5, and 8.8 wt% in the final phosphorescent copolymers. Based on the feed ratios between **MC** and **IrM2**, the obtained copolymers are named **P-RC-1** ($m : n = 193 : 5$), **P-RC-2** ($m : n = 183 : 13$), **P-RC-3** ($m : n = 172 : 20$), and **P-RC-4** ($m : n = 162 : 27$), respectively (Fig. 2).

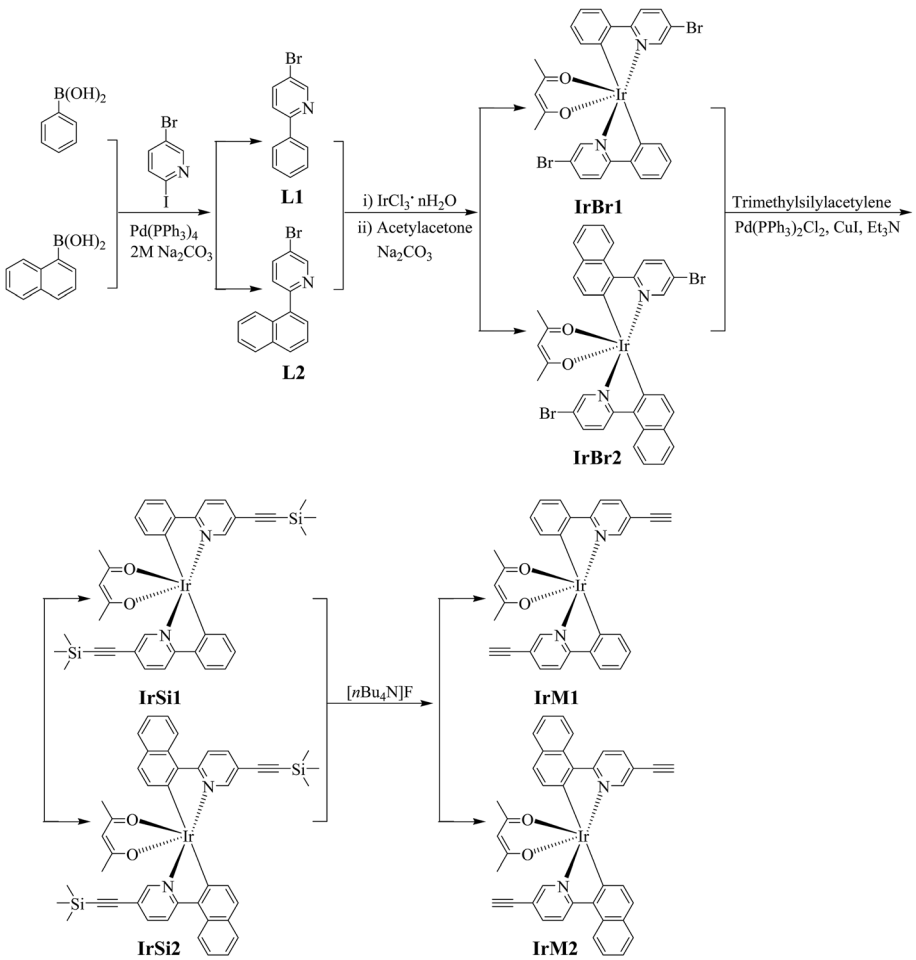

Fig. 1 The synthetic pathways for the phosphorescent monomers.

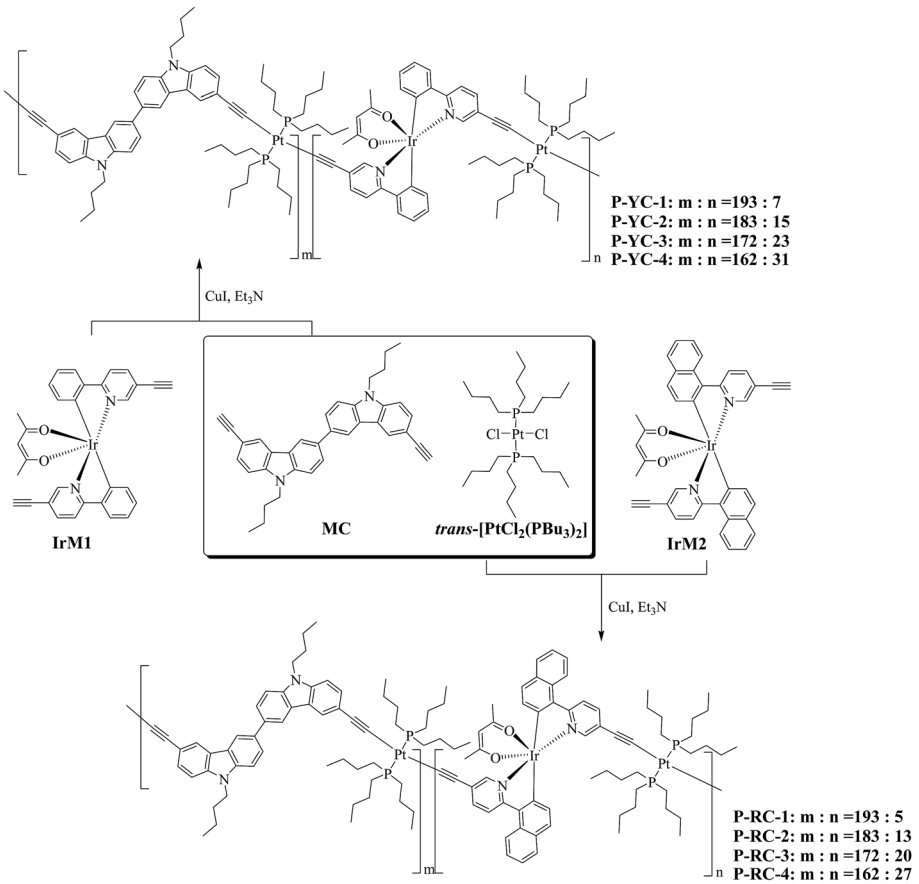

Fig. 2 The synthetic protocol for the phosphorescent copolymers.

The platinum(II) polymetallayne **P-BC** was also prepared through Sonogashira cross-coupling between **MC** and *trans*-$[PtCl_2(PBu_3)_2]$ (Scheme S1†) as a model polymer. In order to investigate the photophysical and electrochemical properties of these phosphorescent copolymers, **P-BC** can properly represent the photophysical and electrochemical behaviours of the backbones in these phosphorescent polymers due to the low content of the Ir^{III} phosphorescent units.

3.2. Thermal characters, photophysical properties and electrochemistry

The thermal properties of these platinum(II) polymetallayne-based phosphorescent copolymers were investigated using thermogravimetric analysis (TGA) and differential scanning calorimetry (DSC) under a nitrogen atmosphere. The TGA results show very good thermal stability of these phosphorescent copolymers with a high 5% weight-reduction temperature ($\Delta T_{5\%}$) ranging from *ca.* 310 °C to 330 °C (Table 1). Furthermore, these phosphorescent copolymers show a good ability in maintaining morphology stability due to their high glass-transition temperatures (T_g) over 150 °C (Table 1), which can be ascribed to their rigid polymetallayne backbone with highly twisted configuration afforded by both bicarbazole and Ir^{III} phosphorescent units. Thus, the good thermal properties will benefit their application in the field of OLEDs. It has been taken for granted that carbon–carbon triple bonds exhibit poor thermal stability disfavoring the application of the concerned compounds in the field of EL. However, recent results have shown that the emitters with carbon–carbon triple bonds can still produce very good EL performances in OLEDs.[31] Hence, the problem associated with the triple-bond containing EL materials should be case by case. In this case, the good thermal properties should guarantee the proper application of these phosphorescent copolymers as emitters in PHOLEDs.

In their UV-Vis absorption spectra (Fig. 3a, b and Table 1), the phosphorescent copolymers possess two kinds of absorption bands. The strong absorption bands located before *ca.* 370 nm can be safely assigned to the bicarbazole-based platinum(II) polymetallayne backbones due to their great resemblance to those of the model polymer **P-BC**. These strong absorption bands should be induced by the metal disturbed π–π* transitions from the bicarbazole units. Clearly, the increasing content of phosphorescent units will lower the amount of bicarbazole blocks in the obtained phosphorescent copolymers. As a result, the strong absorption bands of these phosphorescent copolymers are weakened (Fig. 3a and b). However, the much weaker absorption bands appear in a long wavelength region with an increasing content of phosphorescent units (*ca.* 440 nm for **P-YC-1–P-YC-4** and *ca.* 506 nm for **P-RC-1–P-RC-4**) (Fig. 3a, b and Table 1). The model polymer **P-BC** exhibits no weak absorption

Table 1 Photophysical and thermal data for the phosphorescent copolymers

Polymers	Absorption λ_{abs}[a] (nm) 298 K	Emission λ_{em}[b] (nm) solution at 298 K/film at 298 K/low temperature at 77 K	$\Delta T_{5\%}/T_g$ (°C)
P-YC-1	261, 294, 325, 342, 440	410(0.22 ns), 555(1.0 μs), 598/556, 597/506, 549(13.0 μs), 597	325/150
P-YC-2	260, 295, 324, 343, 440, 478	410(0.21 ns), 555(0.9 μs), 597/556, 597/506, 550(13.7 μs), 597	334/155
P-YC-3	262, 294, 325, 343, 441, 479	412(0.18 ns), 555(0.8 μs), 597/556, 597/506, 550(12.0 μs), 597	341/157
P-YC-4	260, 294, 323, 345, 440, 480	412(0.19 ns), 555(0.8 μs), 598/558, 597/506, 551(11.3 μs), 507	348/159
P-RC-1	260, 294, 324, 343, 505	425(0.22 ns), 632(0.8 μs), 688/630, 683/458, 539, 626(21.4 μs), 685	312/155
P-RC-2	260, 294, 324, 343, 478, 506	426(0.21 ns), 632(0.9 μs), 688/630, 683/457, 539, 628(20.1 μs), 686	311/153
P-RC-3	261, 295, 324, 342, 478, 506	429(0.18 ns), 632(0.7 μs), 688/633, 687/456, 540, 627(19.9 μs), 685	313/155
P-RC-4	261, 294, 324, 343, 478, 506	429(0.19 ns), 632(0.7 μs), 688/635, 685/456, 540, 629(19.0 μs), 687	320/160
P-BC	257, 293, 323, 345	420(0.22 ns)/424/456(29.6 μs), 481, 504	330/145

[a] Measured in CH_2Cl_2 at a concentration of 0.02 mg mL^{-1}. [b] Measured in CH_2Cl_2 at a concentration of 0.02 mg mL^{-1}. The lifetimes in the parentheses are provided behind the corresponding emission band. The excitation wavelength for the measure was set at 360 nm.

bands at a long wavelength. Clearly, these inconspicuous absorption bands with very low intensity should be assigned to the metal-to-ligand charge transfer states for both singlet (^{1}MLCT) and triplet (^{3}MLCT) from the Ir^{III} phosphorescent units (Fig. 3a, b and Table 1). Due to the low content of the Ir^{III} phosphorescent units in the copolymers, the π–π* transition absorption from their organic ligands should give an inessential contribution to the strong absorption bands of the copolymers.

The photoluminescent (PL) spectra for the two series of phosphorescent copolymers are recorded in CH_2Cl_2 solution with the excitation wavelength at 360 nm (Fig. 3c, d and Table 1). For the copolymers **P-YC-1–P-YC-4**, the predominant yellow phosphorescent emission band at *ca.* 555 nm can be observed (Fig. 3c and Table 1), while the copolymers **P-RC-1–P-RC-4** produce a red emission band at *ca.* 632 nm. All these emission bands should be induced by the Ir^{III} phosphorescent centers in the polymer backbone due to their microsecond lifetime (Table 1). The intensity of these phosphorescent bands is enhanced with the increasing content of the Ir^{III} phosphorescent units. Apart from the phosphorescent emission bands located in the long wavelength region, these copolymers also show a high-energy emission band (Fig. 3c, d and Table 1). According to their nanosecond lifetime (*ca.* 0.2 ns) together with the PL spectrum of the model polymer **P-BC** (Table 1 and Fig. 3b), these high-energy emission bands should be induced by the singlet states of the bicarbazole-based polymetallayne segments in the copolymers. It is worth noting that these novel phosphorescent copolymers can exhibit strong phosphorescent emission even in solution (Fig. 3c and d). Alternatively, the traditional conjugated phosphorescent polymers typically give dominating high-energy emissions from the singlet states of the backbones,

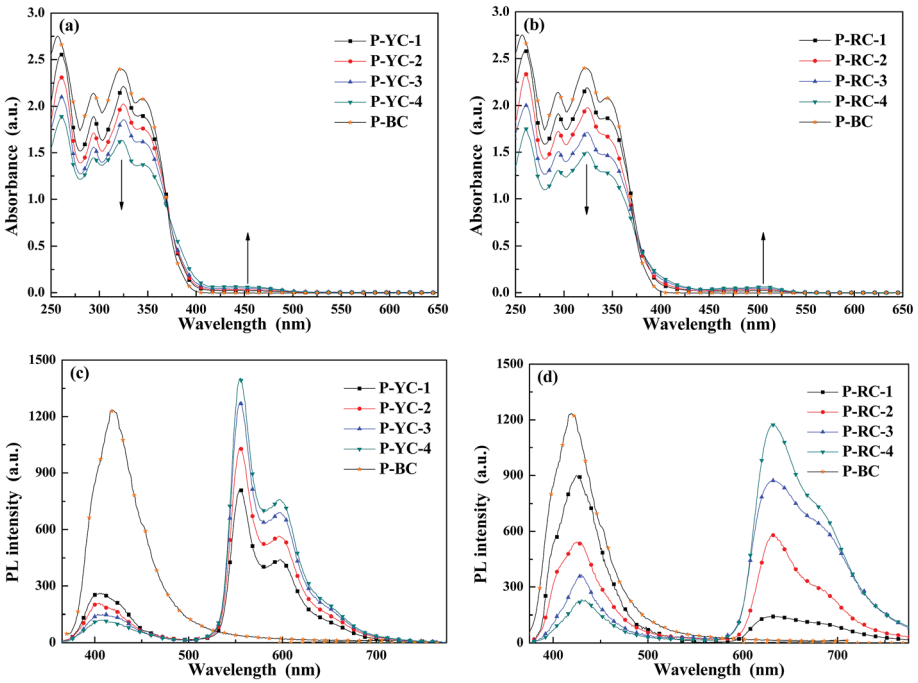

Fig. 3 The absorption and photoluminescent spectra for the CH_2Cl_2 solutions of the phosphorescent polymers at 298 K.

while very weak or even no phosphorescent signal can be detected in solution. Clearly, there should be a much more efficient energy-transfer process involved in these phosphorescent polymers, which should be incurred by the polymetallayne backbones. Obviously, if there is only an energy-transfer process from the singlet states of the polymetallayne backbones to the Ir^{III} phosphorescent units, these copolymers should show similar PL behaviors in the solution to that of the traditional conjugated phosphorescent polymers. Hence, the most likely efficient energy-transfer process involved should come from the triplet states of the polymetallayne backbones, representing their most significant difference from the organic conjugated backbones. If the expected efficient energy-transfer process from the triplet states of the polymetallayne backbones to the Ir^{III} phosphorescent units do happen, the phosphorescent signal associated with the bicarbazole-based polymetallayne backbones should be effectively quenched. In addition, the lifetimes of the phosphorescent band from the Ir^{III} phosphorescent units in these copolymers should be longer than those of the corresponding free phosphorescent monomers **IrM1** and **IrM2**. In order to confirm this issue, the low temperature PL spectra at 77 K for both phosphorescent copolymers and model polymer **P-BC** (Fig. 4) were obtained together with the excited-state lifetimes. Even with low content of the Ir^{III} phosphorescent units (<9 wt%), the phosphorescent signal at *ca.* 460 nm from the polymetallayne backbones can be effectively quenched with respect to that of the model polymer **P-BC**. Furthermore, the phosphorescent lifetimes (τ_p) of the phosphorescent copolymers are also compared with those of the phosphorescent monomers. At 298 K in degassed CH_2Cl_2, the τ_p corresponding to the phosphorescent band at *ca.* 555 nm for **P-YC-1–P-YC-4** is about 1.0 μs, which is much longer than that of the corresponding phosphorescent monomer **IrM1** (0.25 μs). At low temperature 77 K in CH_2Cl_2 glass, **P-YC-1–P-YC-4** show τ_p *ca.* 12 μs for the phosphorescent band from the Ir^{III} phosphorescent units, much longer than that of the phosphorescent monomer **IrM1** (3.1 μs) as well. Furthermore, the low temperature τ_p for **P-YC-1–P-YC-4** is quite close to that of the model polymer **P-BC**. Similar results are obtained for the copolymers **P-RC-1–P-RC-4**: τ_p *ca.* 1.0 μs for **P-RC-1–P-RC-4** *vs.* τ_p *ca.* 0.3 μs for **IrM2** at 298 K; τ_p *ca.* 20 μs for **P-RC-1–P-RC-4** *vs.* τ_p *ca.* 2.7 μs for **IrM2** at 77 K. The lifetime data together with the PL spectra at 77 K clearly indicate that the energy-transfer process from the triplet states of the polymetallayne backbones to the Ir^{III} phosphorescent centers in these novel phosphorescent polymers. Obviously, this new efficient energy-transfer process should be absent in the traditional conjugated phosphorescent polymer solutions under photo-excitation, since the pure organic conjugated backbones prefer to generate singlet excited states rather than triplet ones in photo-excitation process.

According to the aforementioned results, together with the UV-vis absorption and PL spectra in Fig. 5, the energy-transfer processes involved in these phosphorescent copolymers can be figured out. Under the excitation of 360 nm light, the polymetallayne backbones of the copolymers will generate the first singlet states (S_1^p) based on the UV-vis absorption spectrum of the model polymer **P-BC** (Fig. 5). Then, there should be a cascade energy-transfer process from S_1^p to ^{1}**MLCT**$^{\mathbf{Y}}$ (singlet states of MLCT in **IrM1**) (Fig. 6a) and ^{1}**MLCT**$^{\mathbf{R}}$ (singlet states of MLCT in **IrM2**) (Fig. 6b), which are converted *via* inter-system crossing (ISC) into emissive ^{3}**MLCT**$^{\mathbf{Y}}$ (triplet states of MLCT in **IrM1**) (Fig. 6a) and ^{3}**MLCT**$^{\mathbf{R}}$ (triplet states of MLCT in **IrM2**) to induce a yellow phosphorescence signal in **P-YC-1–P-YC-4** and a red phosphorescence signal in **P-RC-1–P-RC-4**, respectively (Fig. 3c and d). This energy-transfer pathway is quite similar to that in conventional phosphorescent polymers with pure organic conjugated backbones. Alternatively, the platinum(II)

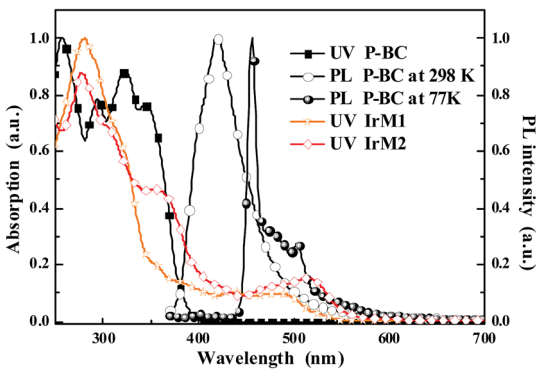

Fig. 5 UV-Vis spectra for the model polymer P-BC and the phosphorescent monomers together with the PL spectrum of P-BC in CH_2Cl_2 at both 298 K and 77 K.

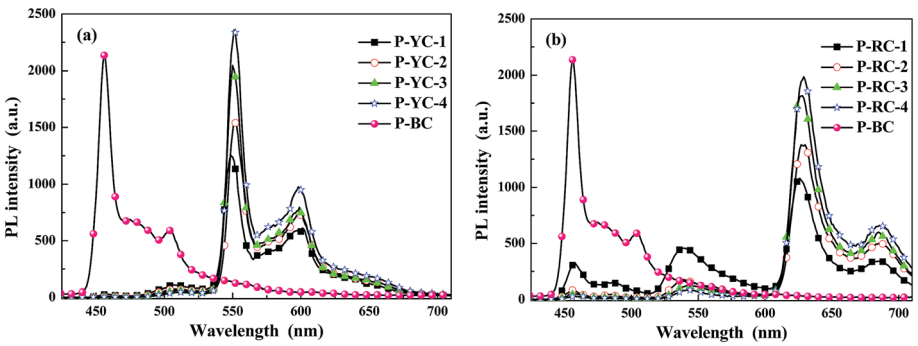

Fig. 4 The photoluminescent (PL) spectra at 77 K for the phosphorescent copolymers and their model polymer P-BC.

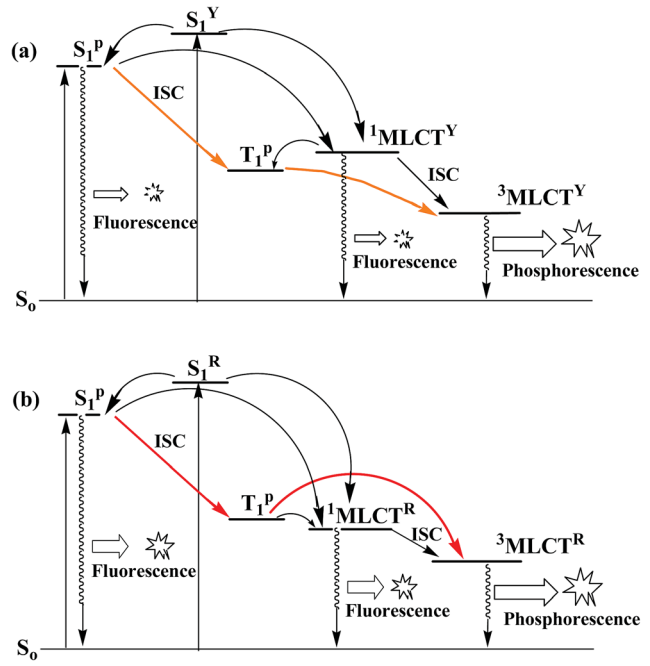

Fig. 6 (a) Energy-transfer sketch involved in the phosphorescent copolymers P-YC-1–P-YC-4. (b) Energy-transfer sketch involved in the phosphorescent copolymers P-RC-1–P-RC-4. S_1^p/T_1^p: singlet/triplet states of the polymetallayne backbones; S_1^Y/S_1^R: singlet sates of the ligands in IrM1/IrM2; $^1MLCT^Y/^3MLCT^Y$: singlet/triplet states of MLCT in IrM1; $^1MLCT^R/^3MLCT^R$: singlet/triplet states of MLCT in IrM2.

ions along the polymetallayne backbones of these copolymers can effectively induce triplet states (T_1^p) from S_1^p through an ISC process, which have confirmed the strong phosphorescent signal in the PL spectrum of the model polymer **P-BC** at 77 K (Fig. 5). Due to the overlap between the MLCT absorption bands of **IrM1**/**IrM2** and the emission bands from T_1^p, the energy-transfer from T_1^p to the emissive ^{3}**MLCT**^{Y}/^{3}**MLCT**^{R} should be very efficient and hence induce a strong yellow phosphorescent emission in **P-YC-1–P-YC-4** (Fig. 6a) and an intense red phosphorescent signal in **P-RC-1–P-RC-4** (Fig. 6b). Thus, it should be due to the efficient energy-transfer from T_1^p to the ^{3}**MLCT** of the phosphorescent centers to induce the strong phosphorescent emission of these copolymers in solution.

Additionally, the organic ligands in the Ir^{III} phosphorescent units in these copolymers can also be excited by the 360 nm light according to the absorption spectra of **IrM1** and **IrM2** (Fig. 5). There should be an energy-transfer process from the singlet sates S_1^Y/S_1^R of the ligands in the yellow/red phosphorescent centers to ^{1}**MLCT**^{Y}/^{1}**MLCT**^{R}, which can be converted into emissive ^{3}**MLCT**^{Y}/^{3}**MLCT**^{R} *via* ISC to induce yellow/red phosphorescence in **P-YC-1–P-YC-4**/**P-RC-1–P-RC-4** as well (Fig. 6a and b). However, this energy-transfer procedure should be inessential compared with the two aforementioned pathways due to the following reasons. Owing to the low content of the phosphorescent Ir^{III} blocks, their ligands will absorb too small an amount of energy from the excitation light to produce a strong phosphorescent signal. Furthermore, possessing a higher energy-level than S_1^p (Fig. 5), S_1^Y/S_1^R can transfer energy to S_1^p, which will not favor the energy-transfer process as well (Fig. 6a and b).

Comparing the PL spectra at both 298 K and 77 K (Fig. 3c *vs.* d and Fig. 4a *vs.* b), the aforementioned energy-transfer processes in **P-YC-1–P-YC-4** should be more efficient than those in **P-RC-1–P-RC-4**, indicated by the much stronger signals for both fluorescence (*ca.* 420 nm) (Fig. 3c *vs.* d) and phosphorescence (*ca.* 460 nm) (Fig. 4a *vs.* b) from the polymetallayne backbones in **P-RC-1–P-RC-4**. From the UV-vis absorption spectra for the phosphorescent monomers and the PL spectrum of **P-BC** at room temperature, the MLCT absorption bands for **IrM1** can show a better overlap with the fluorescent emission band of **P-BC** than that of **IrM2** (Fig. 5), which should guarantee a more efficient energy-transfer from S_1^p to the phosphorescent units in **P-YC-1–P-YC-4**. Thus, the copolymers **P-YC-1–P-YC-4** exhibit much weaker fluorescence signals from the polymetallayne backbones than **P-RC-1–P-RC-4** (Fig. 3c *vs.* d). In addition, the absorption maximum (*ca.* 510 nm) of the ^{3}MLCT band of **IrM2** also deviates far from the predominate phosphorescent emission band (*ca.* 460 nm) of **P-BC** with respect to that of **IrM1** (*ca.* 480 nm for the ^{3}MLCT absorption band) (Fig. 5). This situation also indicates the less efficient energy-transfer from T_1^p to the phosphorescent units in **P-RC-1–P-RC-4**. Accordingly, the phosphorescent signal from the polymetallayne backbones in **P-RC-1–P-RC-4** is also relatively stronger than that of **P-YC-1–P-YC-4** (Fig. 4a *vs.* b).

In the low-temperature PL spectra of these novel phosphorescent copolymers (Fig. 4), there are also weaker high-energy emission bands (*ca.* 505 nm for **P-YC-1–P-YC-4** and *ca.* 540 nm for **P-RC-1–P-RC-4**). Obviously, compared with the PL spectrum of **P-BC** at 77 K (Fig. 4), these weak emission bands should come from the phosphorescent units rather than the polymetallayne backbones of the phosphorescent copolymers. In the PL spectra of **IrM1** and **IrM2** at 77 K, there are weak high-energy emission bands (*ca.* 500 nm for **IrM1** and *ca.* 548 nm for **IrM2**), which should come from the fluorescent emission of the ^{1}MLCT (Fig. S1†). These weak emission bands possess quite similar wavelengths to those of the high-energy emission in the phosphorescent copolymers previously mentioned. Hence, high-energy emission bands *ca.* 505 nm for **P-YC-1–P-YC-4** and *ca.* 540 nm for **P-RC-1–P-RC-4** can be assigned to the emission of the ^{1}MLCT states from the phosphorescent units. According to the UV-vis absorption spectrum of **IrM1** (Fig. 5), the absorption for lowest ^{1}**MLCT**^{Y} states of the phosphorescent units in **P-YC-1–P-YC-4** should be *ca.* 436 nm, corresponding to the energy-level of 2.84 eV. This energy-level is higher than the triplet states of the polymetallayne backbones (T_1^p *ca.* 2.73 eV), which can promote energy-transfer from ^{1}**MLCT**^{Y} to T_1^p. Clearly this energy-transfer process will reduce the population of ^{1}**MLCT**^{Y} excited states, which will reduce their chance of decay to the ground states radiatively (Fig. 5). Hence, the concerned emission band at *ca.* 505 nm is very weak for **P-YC-1–P-YC-4** (Fig. 4a). On the contrary, the situation is different in **P-RC-1–P-RC-4**. The energy-level of the ^{1}**MLCT**^{R} states is *ca.* 2.62 eV corresponding to *ca.* 473 nm (Fig. 5), which is a lower T_1^p (*ca.* 2.73 eV). Thus, there should be an energy-transfer from T_1^p to ^{1}**MLCT**^{R}, which will increase the population of the ^{1}**MLCT**^{R}

states in the excitation process of **P-RC-1–P-RC-4** to enhance their radiative decay to the ground states. Accordingly, the emission band from ^{1}**MLCT**^{R} in **P-RC-1–P-RC-4** is enhanced (Fig. 4b).

3.3. Electrochemical characterization

The electrochemical properties of the two series of phosphorescent copolymers were characterized through cyclic voltammetry (CV) experiments under nitrogen atmosphere with ferrocene (Fc) as the standard. All the phosphorescent copolymers possess a quasi-irreversible oxidation process in the potential range from *ca.* 0.33 V to 0.36 V *vs.* Fc/Fc^{+} (Table 2). Based on the CV results for the Ir^{III} ppy-type phosphorescent complexes, the reduction waves for the *N*-heterocycle aromatic moieties can be detected. However, no detectable reduction procedure has been recorded for these phosphorescent copolymers. This result can be ascribed to the low content of the Ir^{III} phosphorescent units in the copolymers and the relevant CV signals cannot be detected properly. With the aim of assigning the origin of the oxidation process, the CV measurement of the model polymer **P-BC** is also carried out. The polymer **P-BC** exhibits E_p at *ca.* 0.33 V, which is quite close to those from the phosphorescent copolymers. Furthermore, the platinum(II) centers typically show an irreversible oxidation process with E_p at *ca.* 0.5 V.[32] Thus, the oxidation peak should be induced by the bicarbazole units in the backbone of the phosphorescent copolymers. Critically, the low oxidation potentials can furnish these phosphorescent copolymers with good hole injection (HI) abilities. Together with the excellent hole-transporting (HT) characters of the carbazole groups,[33] these phosphorescent copolymers exhibit good hole injection/transporting (HI/HT) properties to enhance their EL performances.

3.4. Electrophosphorescence characterization

As mentioned previously, there is efficient energy-transfer from the triplet states of the polymetallayne backbone to the Ir^{III} phosphorescent units in these novel phosphorescent copolymers. This should represent very important characteristics of these copolymers, as the triplet energy-transfer process can play a critical role in the operation of the PHOLEDs. Even for PHOLEDs based on traditional conjugated phosphorescent copolymers, there is also a predominant energy-transfer process from the triplet states of the conjugated backbones to the phosphorescent units in the EL process.[18] Thus, the unique energy-transfer processes aforementioned in these novel phosphorescent copolymers should benefit their EL process. Additionally, due to the weak conjugation-extending ability of the platinum(II) ions,[26,27,29,34,35] the polymetallayne backbones of these copolymers can exhibit a high triplet energy-level (*ca.* 2.73 eV) to effectively block the reverse energy-transfer process. Furthermore, the phosphorescent copolymers possess a good film-forming ability indicated by the low root mean square (RMS) roughness of *ca.* 2.0 nm (Fig. S2†). With all the features together with the HI/HT ability afforded by the bicarbazole moieties, these novel phosphorescent copolymers should show great potential in PHOLEDs. Their EL capacity has therefore been characterized.

The solution-processed PHOLEDs based on these copolymers were fabricated with the configuration of ITO/PEDOT:PSS (45 nm)/emission layer, EML (35 nm)/TPBi (45 nm)/LiF (1 nm)/Al (100 nm) (Fig. 7). The PEDOT:PSS layer acts as a hole-injection layer (HIL). The 1,3,5-tris(1-phenyl-1*H*-benzo[*d*]-imidazol-2-yl)benzene (TPBi) layer plays the role of both hole-blocking and electron-transporting, while LiF serves as an electron-injection layer. When proper voltage was applied to the these PHOLEDs, intense yellow electrophosphorescence at *ca.* 550 nm can be observed from the devices Y1–Y4 with **P-YC-1–P-YC-4** as the emitter, while red electrophosphorescence at *ca.* 630 nm can be detected from devices R1–R4 with **P-RC-1–P-RC-4** as the emitter (Fig. 8). All the devices show EL representing a similar line-shape to that of corresponding copolymers in solid film (Fig. S3†), indicating that the origin of the EL is from the phosphorescent units. The enhanced long-wavelength band in the EL spectra of the red-emitting PHOLEDs, especially for

Table 2 Redox properties of the copolymers

Copolymers	E_p (V)	E_g[a] (eV)	E_{HOMO} (eV)	E_{LUMO}[b] (eV)
P-YC-1	0.33	3.15	−5.13	−1.98
P-YC-2	0.33	3.15	−5.13	−1.98
P-YC-3	0.35	3.14	−5.15	−2.01
P-YC-4	0.36	3.09	−5.16	−2.07
P-RC-1	0.33	3.18	−5.13	−1.95
P-RC-2	0.34	3.06	−5.14	−2.08
P-RC-3	0.35	3.05	−5.15	−2.10
P-RC-4	0.35	3.05	−5.15	−2.10
P-BC	0.33	3.20	−5.13	−1.93

[a] Obtained through the onset of the UV-vis absorption spectra. [b] $E_{LUMO} = E_{HOMO} + E_g$.

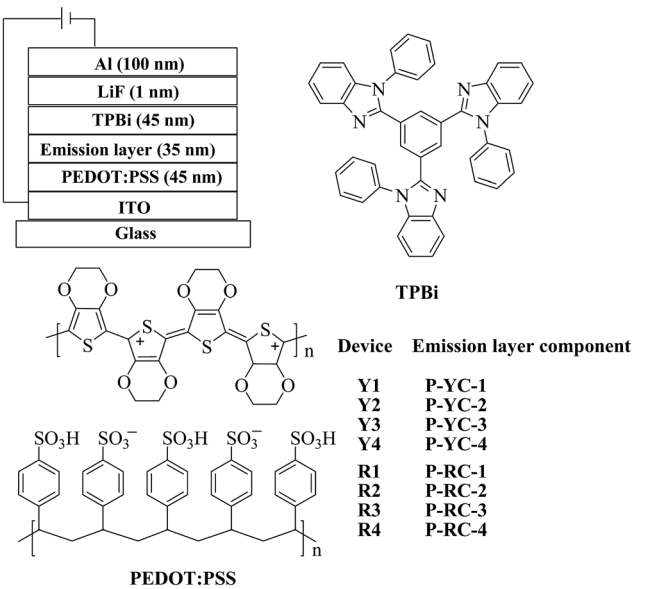

Fig. 7 The configuration of the PHOLEDs made from the phosphorescent copolymers, and the chemical structures for the involved functional materials.

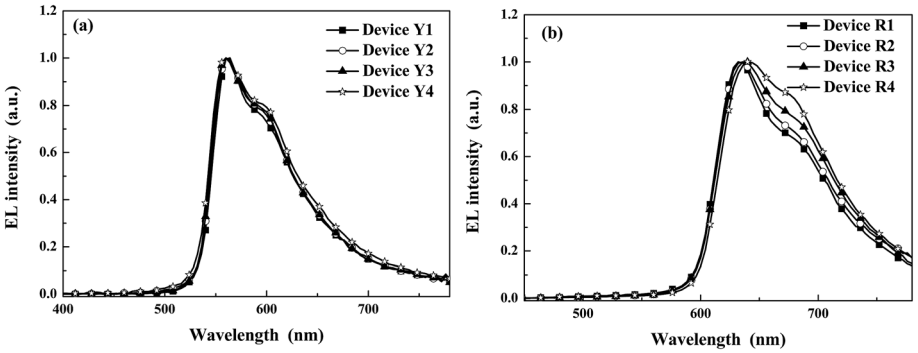

Fig. 8 (a) The EL spectra of devices Y1–Y4 at *ca.* 12 V. (b) The EL spectra of devices R1–R4 at *ca.* 12 V.

device R4, should be induced by the aggregation amongst the phosphorescent units in different polymer backbones. No obvious EL bands from the polymetallayne backbones of the copolymers can be detected (Fig. 8), indicating the complete energy-transfer in the EL processes of these phosphorescent copolymers. This result should be ascribed to the high triplet energy-level of the bicarbazole-based polymetallayne backbones and the highly efficient triplet energy-transfer process mentioned previously (Fig. 6a and b), indicating the crucial role played by the polymetallayne backbones in the EL process of the concerned phosphorescent copolymers.

The current-density–voltage–luminance (*J*–*V*–*L*) curves for the PHOLEDs are shown in Fig. 9 and S4.† The corresponding EL data are summarized in Table 3. Among all the yellow-emitting solution-processed PHOLEDs, device Y3 shows the highest EL performances with a peak luminance (L_{max}) of 5677 cd m^{-2} at 12.3 V, a current efficiency (η_L) of 11.49 cd A^{-1}, an external quantum efficiency (η_{ext}) of 4.38% and a power efficiency (η_P) of 3.78 lm W^{-1} (Fig. 9b and Table 3). With L_{max} of 2418 cd m^{-2} at 14.6 V, η_L of 5.86 cd A^{-1}, η_{ext} of 10.1% and η_P of 2.29 lm W^{-1}, device R2 represents the best red-emitting PHOLED achieved by these phosphorescent copolymers (Fig. 9d and Table 3). Even at a high L_{max} of 1000 cd m^{-2}, device Y3 and R2 can still produce attractive EL efficiencies of 10.64 cd A^{-1} and 4.87 cd A^{-1}, respectively (Table 3). Besides device Y3 and R2, other devices can also show good EL performances, such as device Y2 (7.55 cd A^{-1}) and R1 (4.02 cd A^{-1}) (Table 3). Clearly, these nice EL performances associated with the

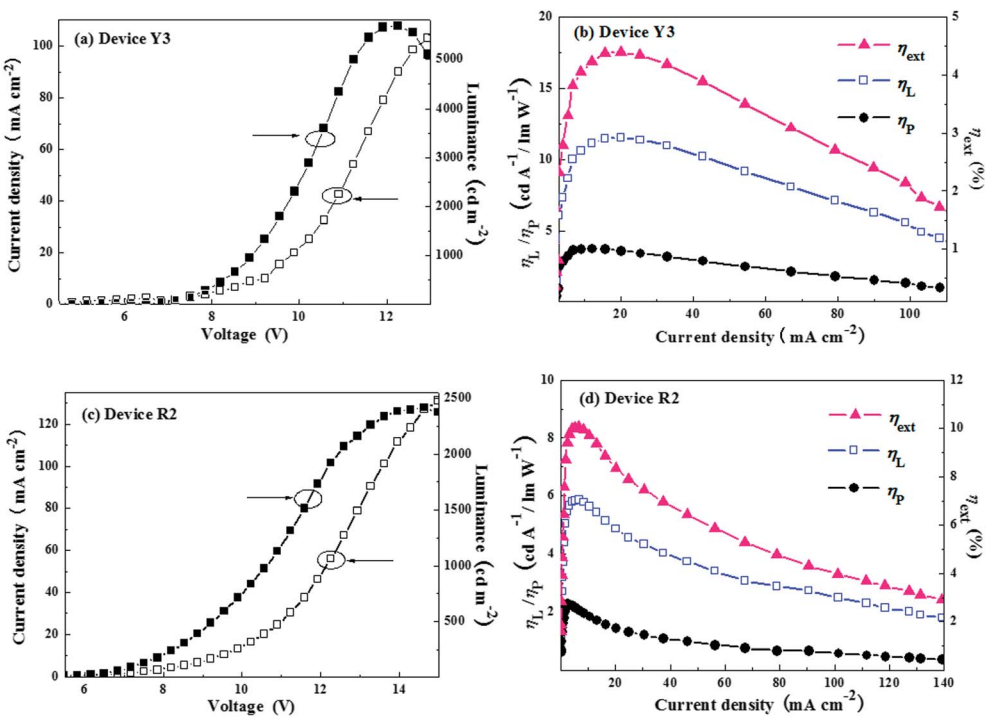

Fig. 9 (a) The current-density–voltage–luminance (*J*–*V*–*L*) curves for device Y3. (b) The relationship between EL efficiency and current density for device Y3. (c) The current-density–voltage–luminance (*J*–*V*–*L*) curves for device R2. (d) The relationship between EL efficiency and current density for device R2.

Table 3 EL performance of the PHOLEDs

Device	Polymers	$V_{turn\text{-}on}$ [V]	Luminance L_{max}[a] [cd m^{-2}]	η_{ext} [%]	η_L [cd A^{-1}]	η_P [lm W^{-1}]	λ_{max}[d] [nm]
Y1	**P-YC-1**	5.5	1682 (12.9)	1.45 (9.55)[a]	3.75 (9.55)	1.26 (8,87)	555 (0.51, 0.48)
				1.27[b]	3.30	1.25	
				1.31[c]	3.42	0.97	
Y2	**P-YC-2**	5.1	3419 (14.0)	2.87 (10.56)	7.55 (10.56)	2.29 (9.89)	555 (0.51, 0.49)
				2.57	5.18	2.07	
				3.32	7.45	2.26	
Y3	**P-YC-3**	4.5	5677 (12.3)	4.38 (9.89)	11.49 (9.55)	3.78 (9.55)	555 (0.51, 0.49)
				1.72	4.52	1.98	
				4.04	10.64	3.77	
Y4	**P-YC-4**	4.5	4251 (13.6)	1.87 (10.23)	4.82 (10.23)	1.62 (8.87)	555 (0.51, 0.49)
				1.33	3.41	1.45	
				1.83	4.72	1.58	
R1	**P-RC-1**	5.8	1738 (15.3)	6.42 (9.21)	4.02 (9.21)	1.49 (8.20)	631 (0.67, 0.32)
				6.20	3.88	1.49	
				4.87	3.05	0.79	
R2	**P-RC-2**	4.5	2418 (14.6)	10.1 (8.87)	5.86 (8.87)	2.29 (7.51)	631 (0.68, 0.32)
				8.69	5.05	2.21	
				8.37	4.87	1.45	
R3	**P-RC-3**	4.0	2057 (15.0)	6.67 (8.29)	3.71 (8.29)	1.65 (5.94)	631 (0.68, 0.32)
				4.42	2.46	1.62	
				5.58	3.10	0.89	
R4	**P-RC-4**	6.5	1453 (18.5)	3.41 (13.15)	1.72 (13.15)	0.43 (12.15)	631 (0.68, 0.32)
				3.00	1.51	0.41	
				2.02	1.19	0.19	

[a] Maximum values of the devices. Values in parentheses are the voltages at which they were obtained. [b] Values were collected at 100 cd A^{-1}. [c] Values collected at 1000 cd A^{-1}. [d] Values were collected at 12 V and CIE coordinates (x, y) are shown in parentheses.

phosphorescent polymers indicate the great potential of these novel phosphorescent polymers with platinum(II) polymetallayne backbones, which have rarely been explored in the field of PHOLEDs.[30] Despite the fact that some functionalized conventional phosphorescent polymers can produce high EL performances,[14,16,36–39] most of them still show relatively low EL efficiencies with a η_L less than 5.0 cd A^{-1}. However, the green-emitting fluorescent OLEDs based on bithiozole-based platinum(II) polymetallaynes just show a η_L of 0.11 cd A^{-1}.[25] Some conjugated orange phosphorescent polymers with oxadiazole moieties exhibit a η_L of 0.61 cd A^{-1}.[40] Through attaching both functional groups and a red-emitting benzothiophene-based Ir^{III} complex to the side chains, the phosphorescent polymer with a non-conjugated backbone has been developed to show η_{ext} of 5.1% and η_P of 3.3 lm W^{-1}.[36] The concerned yellow phosphorescent copolymers can even show higher EL efficiency (11.49 cd A^{-1}) than that of our recently developed analogs (9.17 cd A^{-1}).[30] Therefore, compared with the documented phosphorescent polymers, these phosphorescent copolymers definitely can show very competitive EL performances, indicating the good potential of the novel polymer skeleton in achieving highly efficient phosphorescent polymers.

4. Conclusion

Through employing bicarbazole-based platinum(II) polymetallayne backbones, novel yellow and red phosphorescent polymers have been successfully developed with ppy-type Ir^{III} complexes as phosphorescent units. Taking the inherent advantages of the platinum(II) polymetallayne, the novel polymer skeletons not only show a high triplet energy-level to block undesired back energy-transfer, but also facilitate highly efficient triplet energy-transfer from the polymetallayne backbone to the Ir^{III} phosphorescent units and enhance the phosphorescent ability. Importantly, the photophysical investigations have revealed the details of the involved triplet energy-transfer process, which would provide important information for further optimization of these novel phosphorescent polymers. Due to these merits, the yellow phosphorescent polymers can produce highly efficient solution-processed PHOLEDs with a η_L of 11.49 cd A^{-1}, η_{ext} of 4.38%, η_P of 3.78 lm W^{-1}, and the red analogs can exhibit very attractive EL performances with a η_L of 5.86 cd A^{-1}, η_{ext} of 10.1%, η_P of 2.29 lm W^{-1}. All of these encouraging results indicate the great potential of these novel phosphorescent polymers in the field of PHOLEDs.

Acknowledgements

This work was financially supported by the Tengfei Project from Xi'an Jiaotong University, the Fundamental Research Funds for the Central Universities, The Program for New Century Excellent Talents in University, the Ministry of Education of China (NECT-09-0651), the Key Creative Scientific Research Team in Shaanxi Province (2013KCT-05), the China Postdoctoral Science Foundation (Grant no. 20130201110034), and the National Natural Science Foundation of China (no. 20902072). The financial support from the State Key Laboratory for Mechanical Behavior of Materials is also acknowledged.

References

1 X. Chen, J.-L. Liao, Y. Liang, M. O. Ahmed, H.-E. Tseng and S.-A. Chen, *J. Am. Chem. Soc.*, 2003, **125**, 636–637.
2 A. J. Sandee, C. K. Williams, N. R. Evans, J. E. Davies, C. E. Boothby, A. Köhler, R. H. Friend and A. B. Holmes, *J. Am. Chem. Soc.*, 2004, **126**, 7041–7048.
3 X. L. Yang, G. J. Zhou and W.-Y. Wong, *J. Mater. Chem. C*, 2014, **2**, 1760–1778.
4 H. Wu, L. Ying, W. Yang and Y. Cao, *Chem. Soc. Rev.*, 2009, **38**, 3391–3400.
5 S. L. Gong, C. L. Yang and J. G. Qin, *Chem. Soc. Rev.*, 2012, **41**, 4797–4807.
6 S. J. Liu, Q. Zhao, Y. Deng, Y. J. Xia, J. Lin, Q. L. Fan, L. H. Wang and W. Huang, *J. Phys. Chem. C*, 2007, **111**, 1166–1175.
7 H. Y. Zhen, C. Luo, W. Yang, W. Y. Song, B. Du, J. X. Jiang, C. Y. Jiang, Y. Zhang and Y. Cao, *Macromolecules*, 2006, **39**, 1693–1700.
8 G. L. Schulz, X. W. Chen, S. A. Chen and S. Holdcroft, *Macromolecules*, 2006, **39**, 9157–9165.
9 K. Zhang, Z. Chen, Y. Zou, C. L. Yang, J. G. Qin and Y. Cao, *Organometallics*, 2007, **26**, 3699–3707.
10 A. J. Sandee, C. K. Williams, N. R. Evans, J. E. Davies, C. E. Boothby, A. Kohler, R. H. Friend and A. B. Holmes, *J. Am. Chem. Soc.*, 2004, **126**, 7041–7048.
11 J. X. Jiang, Y. H. Xu, W. Yang, R. Guan, Z. Q. Liu, H. Y. Zhen and Y. Cao, *Adv. Mater.*, 2006, **18**, 1769–1773.
12 Z. H. Ma, J. Q. Ding, B. H. Zhang, C. Y. Mei, Y. X. Cheng, Z. Y. Xie, L. X. Wang, X. B. Jing and F. S. Wang, *Adv. Funct. Mater.*, 2010, **20**, 138–146.
13 D. A. Poulsen, B. J. Kim, B. Ma, C. S. Zonte and J. M. J. Frechet, *Adv. Mater.*, 2010, **22**, 77–82.
14 S. Y. Shao, J. Q. Ding, L. X. Wang, X. B. Jing and F. S. Wang, *J. Mater. Chem.*, 2012, **22**, 24848–24855.
15 S. Y. Shao, J. Q. Ding, L. X. Wang, X. B. Jing and F. S. Wang, *J. Am. Chem. Soc.*, 2012, **134**, 20290–20293.
16 Z. H. Ma, L. C. Chen, J. Q. Ding, L. X. Wang, X. B. Jing and F. S. Wang, *Adv. Mater.*, 2011, **23**, 3726–3729.
17 T. Fei, G. Cheng, D. Hu, W. Dong, P. Lu and Y. Ma, *J. Polym. Sci., A: Polym. Chem.*, 2010, **48**, 1859–1865.
18 M. Lian, Y. Yu, J. Zhao, Z. Huang, X. L. Yang, G. J. Zhou, Z. X. Wu and D. D. Wang, *J. Mater. Chem. C*, 2014, **2**, 9523–9525.
19 J. Zhao, M. Lian, Y. Yu, X. G. Yan, X. B. Xu, X. L. Yang, G. J. Zhou and Z. X. Wu, *Macromol. Rapid Commun.*, 2015, **36**, 71–78.
20 G. L. Tu, C. Y. Mei, Q. G. Zhou, Y. X. Cheng, Y. H. Geng, L. X. Wang, D. G. Ma, X. B. Jing and F. S. Wang, *Adv. Funct. Mater.*, 2006, **16**, 101–106.
21 G. J. Zhou, W. Y. Wong, S. Y. Poon, C. Ye and Z. Y. Lin, *Adv. Funct. Mater.*, 2009, **19**, 531–544.
22 G. J. Zhou and W. Y. Wong, *Chem. Soc. Rev.*, 2011, **40**, 2541–2566.
23 W. Y. Wong, X. Z. Wang, Z. He, K. K. Chan, A. B. Djurisic, K. Y. Cheung, C. T. Yip, A. M. C. Ng, Y. Y. Xi, C. S. K. Mak and W. K. Chan, *J. Am. Chem. Soc.*, 2007, **129**, 14372–14380.
24 W. Y. Wong, X. Z. Wang, Z. He, A. B. Djurisic, C. T. Yip, K. Y. Cheung, H. Wang, C. S. K. Mak and W. K. Chan, *Nat. Mater.*, 2007, **6**, 521–527.
25 W. Y. Wong, G. J. Zhou, Z. He, K. Y. Cheung, A. M. C. Ng, A. B. Djurisic and W. K. Chan, *Macromol. Chem. Phys.*, 2008, **209**, 1319–1332.
26 G. J. Zhou, W. Y. Wong, C. Ye and Z. Y. Lin, *Adv. Funct. Mater.*, 2007, **17**, 963–975.
27 G. J. Zhou, W. Y. Wong, Z. Y. Lin and C. Ye, *Angew. Chem., Int. Ed.*, 2006, **45**, 6189–6193.
28 M. S. Khan, M. R. A. Al-Mandhary, M. K. Al-Suti, A. K. Hisahm, P. R. Raithby, B. Ahrens, M. F. Mahon, L. Male, E. A. Marseglia, E. Tedesco, R. H. Friend, A. Kohler, N. Feeder and S. J. Teat, *J. Chem. Soc., Dalton Trans.*, 2002, 1358–1368.
29 W.-Y. Wong and C.-L. Ho, *Coord. Chem. Rev.*, 2006, **250**, 2627–2690.
30 Z. Huang, B. A. Liu, J. Zhao, Y. He, X. G. Yan, X. B. Xu, G. J. Zhou, X. L. Yang and Z. X. Wu, *RSC. Adv.*, 2015, **5**, 12100–12110.
31 T. Peng, G. F. Li, Y. Liu, Y. Wu, K. Q. Ye, D. D. Yao, Y. Yuan, Z. M. Hou and Y. Wang, *Org. Electron.*, 2011, **12**, 1068–1072.
32 P.-I. Kvam, M. V. Puzyk, K. P. Balashev and J. Songstad, *Acta Chem. Scand.*, 1995, **49**, 335–343.
33 J. Ding, B. Zhang, J. Lü, Z. Xie, L. Wang, X. Jing and F. Wang, *Adv. Mater.*, 2009, **21**, 4983–4986.
34 S. J. Davies, B. F. Johnson, M. S. Khan and J. Lewis, *J. Chem. Soc., Chem. Commun.*, 1991, **3**, 187–188.
35 N. J. Long and C. K. Williams, *Angew. Chem., Int. Ed.*, 2003, **42**, 2586–2617.
36 J. H. Park, T.-W. Koh, J. Chung, S. H. Park, M. Eo, Y. Do, S. Yoo and M. H. Lee, *Macromolecules*, 2013, **46**, 674–682.
37 W.-Y. Lai, J. W. Levell, M. N. Balfour, P. L. Burn, S.-C. Lo and I. D. Samuel, *Polym. Chem.*, 2012, **3**, 734–740.
38 F. I. Wu, X. H. Yang, D. Neher, R. Dodda, Y. H. Tseng and C. F. Shu, *Adv. Funct. Mater.*, 2007, **17**, 1085–1092.
39 C. H. Chien, S. F. Liao, C. H. Wu, C. F. Shu, S. Y. Chang, Y. Chi, P. T. Chou and C. H. Lai, *Adv. Funct. Mater.*, 2008, **18**, 1430–1439.
40 W. Zhang, H. Jin, F. Zhou, Z. Shen, D. Zou and X. Fan, *J. Polym. Sci., Part A: Polym. Chem.*, 2012, **50**, 3895–3903.